



## Gold boosts nitrate reduction and deactivation resistance to indium-promoted palladium catalysts

Sujin Guo <sup>a,b,1</sup>, Hao Li <sup>c,1</sup>, Kimberly N. Heck <sup>b,d</sup>, Xinying Luan <sup>b,d</sup>, Wenhua Guo <sup>e</sup>, Graeme Henkelman <sup>c,\*</sup>, Michael S. Wong <sup>a,b,d,f,g,\*\*</sup>

<sup>a</sup> Department of Civil & Environmental Engineering, USA

<sup>b</sup> Nanosystems Engineering Research Center for Nanotechnology-Enabled Water Treatment, Rice University, 6100 S. Main Street, Houston, TX 77005, USA

<sup>c</sup> Department of Chemistry and the Oden Institute for Computational Engineering and Sciences, The University of Texas at Austin, 105 E. 24th Street, Stop A5300, Austin, TX 78712, USA

<sup>d</sup> Department of Chemical and Biomolecular Engineering, Rice University, 6100 S. Main Street, Houston, TX 77005, USA

<sup>e</sup> Shared Equipment Authority (SEA), USA

<sup>f</sup> Department of Chemistry, USA

<sup>g</sup> Department of Materials Science and NanoEngineering, Rice University, 6100 S. Main Street, Houston, TX 77005, USA



### ARTICLE INFO

#### Keywords:

Nitrate reduction  
Trimetallic catalysts  
Deactivation resistance  
Gold, palladium

### ABSTRACT

In-decorated PdAu catalysts were synthesized and investigated for the aqueous reduction of nitrate. We first synthesized PdAu nanoparticles (NPs) with varying Pd:Au ratios onto which we deposited In. These In-on-PdAu NPs showed higher activity than In-on-Pd NPs for  $\text{NO}_3^-$  ( $k_{\text{cat}}=4.0\text{--}7.2$  vs  $2.7 \text{ L/g}_{\text{total(Pd+In)}}/\text{min}$ ) due to electronic and ensemble effects. Au-rich NPs had lower activity ( $k_{\text{cat}}=1.3\text{--}1.5 \text{ L/g}_{\text{total(Pd+In)}}/\text{min}$ ) due to unfavorable hydrogen and nitrate/nitrite binding energies. In-on-PdAu NPs showed higher  $\text{N}_2$  selectivity than In-on-Pd NPs (90 % vs 60% at 40% conversion), and had higher activity for  $\text{NO}_2^-$ . Density functional theory calculations suggest that Au weakens metal-N bonding which enables nitrite reduction over Pd. Nitrate reduction is promoted by greater mobility of H-adatoms to regenerate  $\text{InO}_x$  and faster spillover of nitrite onto PdAu. When challenged with species found in drinking water, the trimetallic NPs were more active than bimetallic NPs (1.0–1.6 vs 0.6  $\text{L/g}_{\text{total(Pd+In)}}/\text{min}$ ). These results expand the prospects of practical catalytic denitrification.

### 1. Introduction

Nitrate ( $\text{NO}_3^-$ ) is one of the most ubiquitous contaminants detected globally in groundwater [1,2]. Groundwater often has low levels of naturally occurring  $\text{NO}_3^-$ , however, there are also many anthropogenic  $\text{NO}_3^-$  sources, such as fertilizer runoff, other agricultural sources, and septic tank leakage [3,4]. Elevated nitrate levels in water can pose both acute and long-term hazards to public health. High levels of nitrate in drinking water are of particular concern for infants and pregnant woman and can cause methemoglobinemia and thyroid damage [5,6] and can lead to the formation of cancer-causing N-nitroso compounds in the human body [7]. This has led to the U.S. Environmental Protection Agency (EPA) to regulate nitrate and its reduced form nitrite ( $\text{NO}_2^-$ ) at a maximum concentration level (MCL) of 10 mg-N/L and 1 mg-N/L,

respectively. The EPA has taken action to reduce risk through supporting reductions in nutrient loads from point and nonpoint sources, strengthening nutrient standards, and providing financial assistance to communities for drinking water treatment [8]. Even though surface water systems that serve more people have improved over time, many groundwater systems remain in violation for longer periods, indicating persistent nitrate problems in drinking water [9].

The most commonly implemented technologies for nitrate removal are anion exchange and reverse osmosis. However, these produce brine waste streams, and sustainable application of these technologies is often limited by a lack of local disposal options and the challenge of increasing salt loads [10,11]. The need for alternative options has driven the drinking water community to develop new technologies that effectively remove nitrate while limiting cost and brine disposal challenges. Studies

\* Corresponding author.

\*\* Corresponding author at: Department of Civil & Environmental Engineering, USA.

E-mail addresses: [henkelman@utexas.edu](mailto:henkelman@utexas.edu) (G. Henkelman), [mswong@rice.edu](mailto:mswong@rice.edu) (M.S. Wong).

<sup>1</sup> These authors contributed equally to the manuscript.

**Table 1**  
Composition of Pd-Au NPs.

Target composition (%)		Composition by ICP-OES (%)		Composition by XPS (%)	
Pd	Au	Pd	Au	Pd	Au
100	0	100	0	100	0
90	10	90	10	88	12
80	20	79	21	78	22
70	30	67	33	69	31
50	50	47	53	42	58
30	70	26	74	39	61
10	90	8	92	26	74

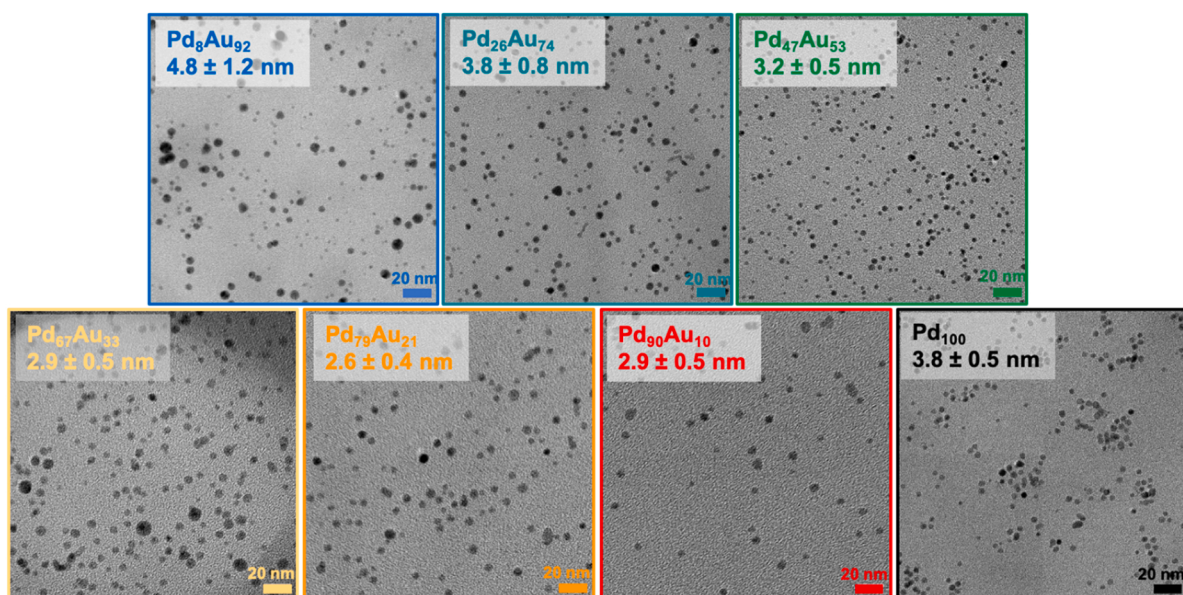


Fig. 1. Representative TEM images of different compositions of Pd-Au alloy core and pure Pd NPs. Scale bars are 20 nm.

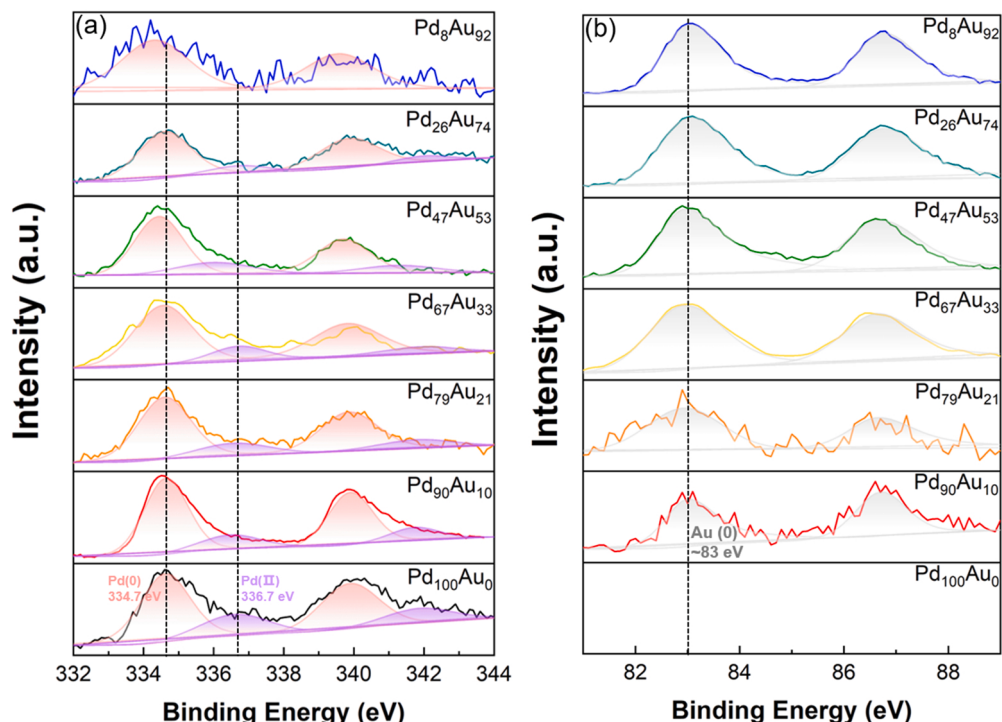


Fig. 2. Pd 3d and Au 4f XPS spectra of different compositions of PdAu catalysts.

**Table 2**

Oxidation state distribution (%) of Pd from all PdAu NPs and In-on-PdAu NPs (derived from XPS data).

Samples	Pd (0) (molar %)	Pd (II) (molar %)	Samples In-on-Pd <sub>x</sub> Au <sub>y</sub>	Pd (0) (molar %)	Pd (II) (molar %)
Pd <sub>8</sub> Au <sub>92</sub>	100	0	In-on-Pd <sub>8</sub> Au <sub>92</sub>	100	0
Pd <sub>26</sub> Au <sub>74</sub>	91	9	In-on-Pd <sub>26</sub> Au <sub>74</sub>	89	11
Pd <sub>47</sub> Au <sub>53</sub>	83	17	In-on-Pd <sub>47</sub> Au <sub>53</sub>	85	15
Pd <sub>67</sub> Au <sub>33</sub>	79	21	In-on-Pd <sub>67</sub> Au <sub>33</sub>	80	20
Pd <sub>79</sub> Au <sub>21</sub>	78	22	In-on-Pd <sub>79</sub> Au <sub>21</sub>	79	21
Pd <sub>90</sub> Au <sub>10</sub>	73	27	In-on-Pd <sub>90</sub> Au <sub>10</sub>	76	24
Pd <sub>100</sub> Au <sub>0</sub>	60	40	In-on-Pd <sub>100</sub> Au <sub>0</sub>	70	30

**Table 3**

Calculated In surface coverage of trimetallic NPs.

Sample	PdAu particle size (nm)	In surface coverage (sc%)
In-on-Pd <sub>8</sub> Au <sub>92</sub>	4.8	25
In-on-Pd <sub>26</sub> Au <sub>74</sub>	3.8	25
In-on-Pd <sub>47</sub> Au <sub>53</sub>	3.2	28
In-on-Pd <sub>67</sub> Au <sub>33</sub>	2.9	27
In-on-Pd <sub>79</sub> Au <sub>21</sub>	2.6	23
In-on-Pd <sub>90</sub> Au <sub>10</sub>	2.9	27
In-on-Pd <sub>100</sub> Au <sub>0</sub>	3.8	25

well as a secondary metal (e.g., In, Cu and Sn) as a promoter [13,16–19]. The most significant obstacle for the nitrate reduction reaction is the identification of a catalytic system that can achieve excellent reaction activity and longevity, while maintaining high selectivity to the desired dinitrogen (N<sub>2</sub>) end-product.

Our previous studies have focused on the synthesis of model In-on-Pd NPs to better understand the “limiting-step” (NO<sub>3</sub> → NO<sub>2</sub>) of NO<sub>3</sub><sup>–</sup> reduction and the reaction mechanism [20–22]. Pd-on-Au NPs [23,24] and mixed Pd-Au alloy catalysts [25] have been studied for direct NO<sub>2</sub><sup>–</sup> reduction, and have shown promotional effects compared with mono-metallic Pd NPs. However, to date they have not been studied as core materials with a promotional metal to further understand the

structure-activity-selectivity relationships for the more difficult NO<sub>3</sub><sup>–</sup> reduction.

The overall goal of this work is to explore the impact of Au on In-decorated Pd catalysis for nitrate/nitrite hydrogenation. To achieve this goal, we designed and synthesized a model catalyst structure with a Pd and Au mixed alloy composition (Pd:Au ratios from 9:1–1:9) in the NP, and with In atoms decorating the NP surface. The resulting In-on-PdAu NPs were evaluated for their NO<sub>3</sub><sup>–</sup> reduction activity in model batch reactions, using H<sub>2</sub> as the electron donor. Catalytic NO<sub>3</sub><sup>–</sup> reduction was also evaluated in simulated drinking water to determine deactivation resistance to common water components. Density functional theory (DFT) was used to assess the NO<sub>2</sub><sup>–</sup> reduction activity over a trimetallic catalytic surface and other reference surfaces by calculating the N and N<sub>2</sub> binding energies, providing plausible explanations for the promotional role of Au. The data obtained allowed us to identify an improved nitrate reduction catalyst design and revealed the importance of the rate-limiting step in the overall reaction.

## 2. Experimental section

### 2.1. Materials

All chemicals were analytical grade and used as received without further purification. Ethylene glycol (EG, 98%), potassium tetrachloroplatinate (II) (K<sub>2</sub>PdCl<sub>4</sub>, 99%), gold(III) chloride trihydrate (HAuCl<sub>4</sub>·3H<sub>2</sub>O, >99.9%), poly(vinylpyrrolidone) (PVP, MW~55,000), indium chloride tetrahydrate (InCl<sub>3</sub>·4H<sub>2</sub>O, 97%), sodium nitrate (NaNO<sub>3</sub>, >99.0%), sodium nitrite (NaNO<sub>2</sub>, >97.0%) and 3-amino-propyl-functionalized silica gel were purchased from Sigma-Aldrich. Nessler reagent was purchased from Fisher-Scientific. Griess reagent was made by dissolving 1.0 g of sulfanilamide (Sigma-Aldrich, ≥98%) and 0.1 g of N-(1-naphthyl)ethylenediamine dihydrochloride (Sigma-Aldrich, >98%) with 2.94 mL H<sub>3</sub>PO<sub>4</sub> (Sigma Aldrich, 85 wt%, 99.99% trace metal basis) in a 100 mL volumetric flask so that the final concentrations are 1 wt% sulfanilamide, 0.1 wt% N-(1-naphthyl)ethylenediamine dihydrochloride and 5% H<sub>3</sub>PO<sub>4</sub>. [26] H<sub>2</sub> and CO<sub>2</sub> gases (99.99% purity) were obtained from Airgas. Nitrate (0.161 M, 10,000 ppm) and nitrite (0.217 M, 10,000 ppm) stock solutions were prepared by dissolving the appropriate amounts of NaNO<sub>3</sub> and NaNO<sub>2</sub> in deionized (DI) water and stored in the dark in a refrigerator at 4 °C. Unless otherwise noted, all experiments were conducted using DI water (> 18 MΩ·cm, Merck Millipore).

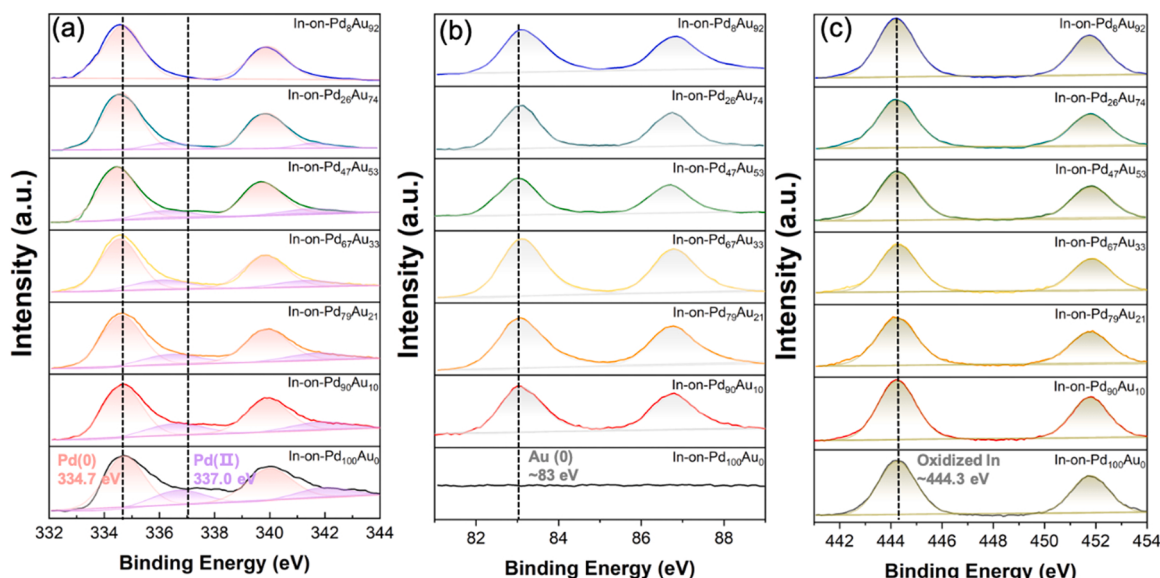
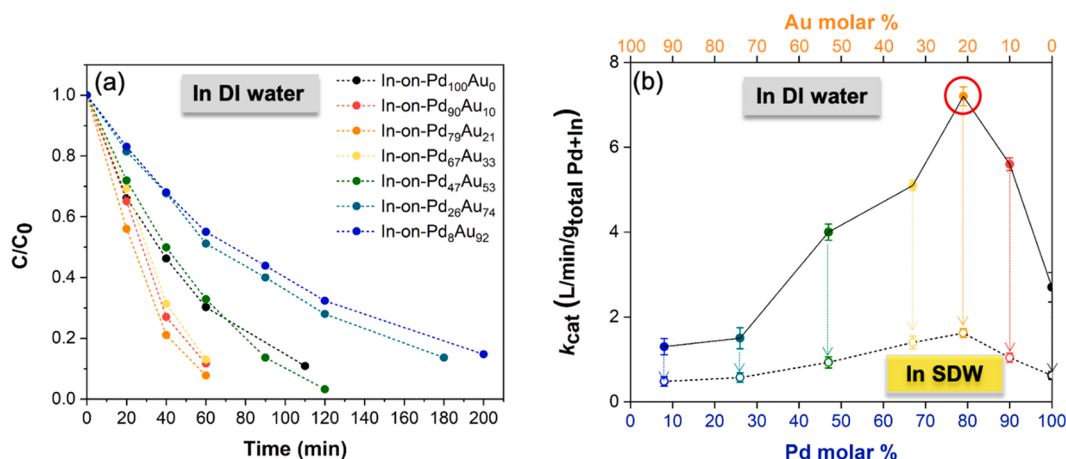


Fig. 3. Pd 3d, Au 4f and In 3d XPS spectra of different compositions of In-on-PdAu NPs.



**Fig. 4.** (a) Nitrate concentration-time profile and (b) pseudo-first order  $\text{NO}_3^-$  reduction reaction rate constants of In-on-PdAu NPs catalyst at varying Pd:Au ratios. Reaction conditions: 350  $\mu\text{g}$  Pd+In loading for In-on-PdAu NPs or In-on-Pd NPs (control sample), 600 rpm stirring rate, 1 atm pressure, 50:50  $\text{H}_2:\text{CO}_2$  pH = 5,  $[\text{NO}_3^-]_0 = 50$  ppm.

## 2.2. Preparation of simulated drinking water (SDW)

SDW contains dissolved species at concentrations typical of drinking water. The SDW composition follows the formulation based on the NSF/ANSI53 standard (Table S1). [27].

## 2.3. Catalyst preparation and characterization

The catalysts used in this work were colloidal NPs synthesized based on previous work [25,28]. Pd-Au alloy NPs were synthesized first as a core material. PVP (200 mg) and NaBH<sub>4</sub> (5.6 equivalents per Au (III) atom) were dissolved in EG (15.0 mL), and the solution temperature was brought to 150 °C under stirring in an oil bath. Separately, the metal precursors (K<sub>2</sub>PdCl<sub>4</sub>; HAuCl<sub>4</sub>·3H<sub>2</sub>O) were each dissolved in EG (2.5 mL) and briefly sonicated to ensure complete dissolution. The exact molar amounts of each metal precursor employed in a given reaction were determined by the target value of x for the Pd<sub>x</sub>Au<sub>100-x</sub> NPs; the combined molar amount of Pd (II) and Au (III) precursors was maintained at 0.10 mmol. The two solutions were then combined and mixed to give a total volume of 5.0 mL, which was delivered directly into the 150 °C PVP/NaBH<sub>4</sub> solution by a 5.0 mL syringe at approximately 0.17 mL/s. After the addition was complete (30 s), the reaction mixture was stirred under constant heating for 5 mins. At the end of the reaction, the reaction flask was quickly cooled using an ice-water bath. The resulting Pd<sub>x</sub>Au<sub>100-x</sub> NPs were precipitated by acetone (40 mL) and isolated by ultracentrifugation (8000 rpm, 20 mins). Pd NPs were also synthesized using the same method but without adding Au precursor and NaBH<sub>4</sub> to the reactor. The NPs were then re-dispersed in 10.0 mL DI water and the concentration and molar ratio between Pd and Au was confirmed via inductively coupled plasma-optical emission spectroscopy (ICP-OES).

The indium precursor (InCl<sub>3</sub>·4H<sub>2</sub>O, 0.04 M) was added successively to the as-synthesized Pd-Au NPs with H<sub>2</sub> bubbled for 30 mins at room temperature, generating the In-on-PdAu NPs. The loading of In was calculated using the magic cluster model [29], with a target goal of adding ~25% surface coverage (sc%) of In to the PdAu NP. In-on-Pd NPs were also synthesized as a reference by reducing the In precursor on the surface of monometallic Pd NPs.

To perform x-ray photoelectron spectroscopy (XPS) measurements, silica powder-immobilized In-on-PdAu NPs were prepared. 10 mg of the PVP-capped In-on-PdAu NPs was mixed with 3-aminopropyl-functionalized silica (Sigma-Aldrich, 40–63  $\mu\text{m}$ ) to achieve a target of approximately 1.5 wt% total metal loading. Typically, the NPs were sonicated for 5 min to ensure a homogeneous dispersion. Separately, silica was added to a 20 mL glass scintillation vial containing a magnetic stir bar. The NP suspension of interest was then added dropwise over 10 min. The

resulting slurry was sonicated for 10 min and stirred overnight, at which point the supernatant was colorless, indicating adsorption of the NPs onto the silica. The supported catalysts were then vacuum filtered in air, washed copiously with water and ethanol, and finally dried overnight in an oven at 40 °C. XPS data was obtained by using a PHI Quantera System with monochromatic Al KR radiation (1486.7 eV).

Transmission electron microscopy (TEM) images were obtained using a JEOL 2010 TEM operating at an accelerating voltage of 200 kV. The particle size distribution was calculated by counting at least 200 particles with ImageJ software.

## 2.4. Catalyst activity characterization

$\text{NO}_3^-$  reduction experiments were conducted at constant temperature (22 ± 1 °C) and atmospheric pressure (1 atm) under magnetic stirring in a septum-sealed glass batch reactor (50 mL). The reaction medium contained source water amended with the prepared catalyst (6.6  $\mu\text{g}/\text{L}$  Pd and 1  $\mu\text{g}/\text{L}$  In) and the suspension was bubbled with  $\text{H}_2$  gas (reductant) and  $\text{CO}_2$  gas (buffer) at equal flowrates (50 mL/min) for 15 min to saturate the water and headspace. The reaction was initiated by injecting 250  $\mu\text{L}$  of NaNO<sub>3</sub> aqueous stock solution (0.161 M) to achieve an initial concentration of 50 ppm of  $\text{NO}_3^-$  (= 50 mg- $\text{NO}_3^-/\text{L}$  ~ 11.3 mg-N/L). The  $\text{CO}_2$  buffer maintained a pH of 5.6–5.8 throughout the reaction. Samples were taken at regular time intervals for analysis; the total sample volume removed was ≤ 10% of the total solution volume. Since the catalyst suspension was homogeneously dispersed in the reactor, the catalyst concentration in the reactor remained approximately constant. Experiments were repeated in triplicate. The kinetic experiments with SDW were performed using a similar method above except the reaction media was SDW instead of DI water. Reactions using nitrite were similarly run as described in DI water, except using a starting concentration of 37 ppm nitrite for an equivalent molar concentration of N as the nitrate reduction experiments.

Nitrite concentrations and ammonium concentrations were analyzed using the Griess and Nessler tests, respectively. The Griess or Nessler reagent solution (0.2 mL), a sample solution (0.2 mL), and water (1.6 mL) were mixed and allowed to react at room temperature for 10 min, after which no further color change was observed. The Griess test resulted in a typical magenta color and the Nessler test had a light yellow color. The absorbance at 540 nm and 480 nm was measured via UV-vis spectroscopy, and the concentrations were determined in the 0–2.0 ppm range using standard calibration curves. Nitrate measurements were made using a nitrate ion selective electrode (Cole-Parmer, lower detection limit 0.1 ppm).

$\text{NO}_3^-$  and  $\text{NO}_2^-$  reduction were found to follow pseudo-first-order

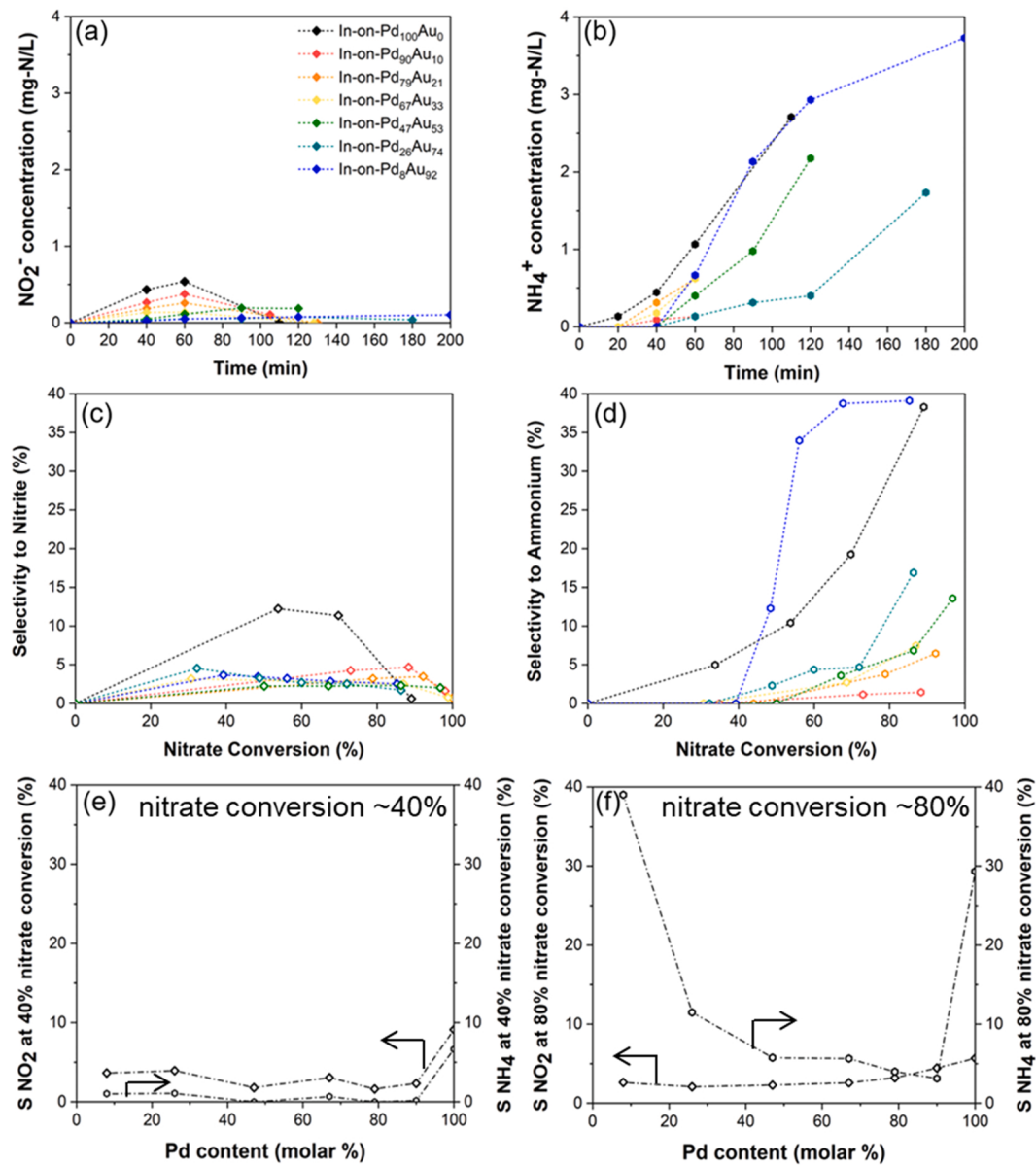


**Fig. 5.** Concentration-time profiles of (a)  $\text{NO}_2^-$  and (b)  $\text{NH}_4^+$  species, and selectivity-conversion plots for (c)  $\text{NO}_2^-$  and (d)  $\text{NH}_4^+$  species, for In-on-PdAu NP compositions including bimetallic In-on-Pd<sub>100</sub>Au<sub>0</sub>. Selectivity to  $\text{NO}_2^-$  and  $\text{NH}_4^+$  species at (e) low and (f) high nitrate conversion.

kinetics for conversion up to and greater than 80% of the initial concentration. The observed first-order rate constants  $k_{\text{obs}}$  were normalized by the total gram amount of active metals (i.e. Pd+In) for each catalyst, obtained from linear regression of the natural log of concentration versus time plots, using equation

$$-\frac{dC_{\text{NO}_3^-}}{dt} \left( \frac{1}{C_{\text{cat}}} \right) = k_{\text{cat}} C_{\text{NO}_3^-}$$

where  $C_{\text{NO}_3^-}$  represents the aqueous nitrate concentration (mg  $\text{NO}_3^-$ /L),  $C_{\text{cat}}$  represents the concentration of total Pd and In metal in the catalyst (g total Pd+In/L), and  $k_{\text{cat}}$  is the observed first-order rate constant normalized by metal concentration (L/min/g total Pd+In).

The initial concentration of nitrate and the concentration of nitrate after time  $t$  are  $C_0$  and  $C$  (mg-N/L). The selectivity to ammonium and selectivity to nitrite are calculated from

$$S_{\text{NH}_4^+} = \left( \frac{C_{\text{NH}_4^+ - N}}{C_0 - C} \right) \times 100\%$$

$$S_{\text{NO}_2^-} = \left( \frac{C_{\text{NO}_2^- - N}}{C_0 - C} \right) \times 100\%.$$

Since prior studies have indicated that only trace amount of intermediate products NO and  $\text{N}_2\text{O}$  were formed [19,30,31], the selectivity to  $\text{N}_2$  was calculated as:

$$S_{\text{N}_2} = 100\% - S_{\text{NH}_4^+} - S_{\text{NO}_2^-}$$

## 2.5. Density functional theory calculations

Density functional theory (DFT) calculations were performed using the VASP code with the Perdew-Burke-Ernzerhof functional and the projector augmented wave method [32,33]. Structural optimizations were carried out using a  $(3 \times 3 \times 1)$   $k$ -point mesh with the method developed by Monkhorst and Pack [34]. Convergence was determined when the force on each atom dropped below 0.05 eV/Å. The kinetic energy cutoff for the plane wave basis was set as 400 eV for all of the calculations. A four-layer,  $(4 \times 4)$  slab was modeled to simulate the

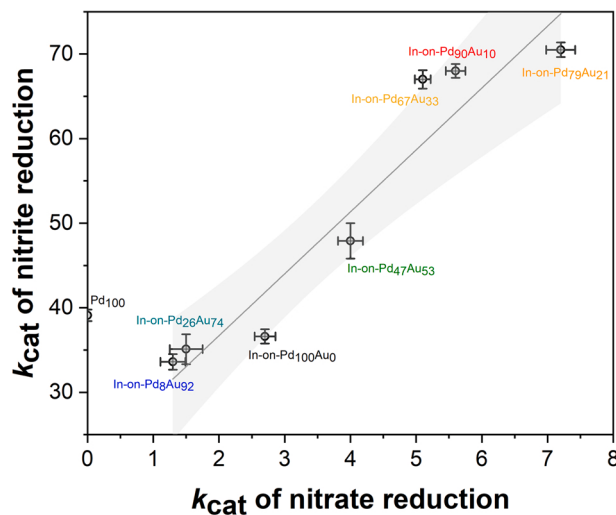


**Fig. 6.** Correlation profile of  $\text{NO}_2^-$  reduction kinetics and  $\text{NO}_3^-$  reduction kinetics. Grey solid line is linear regression of  $k_{\text{cat}}(\text{NO}_2^-)$  versus  $k_{\text{cat}}(\text{NO}_3^-)$  for each sample, and enclosed grey region represent 95% confidence intervals of linear regression. Kinetics unit:  $\text{L/g}_{\text{total Pd+In}}/\text{min}$ .

catalytic surface, with the upper two layers allowed to relax, while the bottom two layers were constrained in bulk positions. A vacuum layer of at least  $12 \text{ \AA}$  was applied in the  $z$ -direction of the slab, to separate periodic images. The  $\text{Pd}_3\text{-In}$ ,  $\text{Pd}_2\text{In}_1$ , and  $\text{Pd}_1\text{In}_2$  ensembles were respectively modeled by replacing 3  $\text{Pd} + 1\text{In}$ , 2  $\text{Pd} + 1\text{In}$ , and 1  $\text{Pd} + 2\text{In}$  with the surface  $\text{Au}$  atoms of a  $\text{Au}(111)$  slab.

### 3. Results and discussion

#### 3.1. Catalyst characterization and optimizing In loading

The calculated and measured values of  $\text{Pd}:\text{Au}$  molar ratios for the  $\text{PdAu}$  alloy core NPs are shown in Table 1. The bulk  $\text{Pd}:\text{Au}$  compositions of the products were examined by ICP-OES and the surface  $\text{Pd}:\text{Au}$  molar ratios were investigated by XPS. The results show that the actual  $\text{PdAu}$  alloy NPs obtained were well matched with the target compositions, with  $\text{Au}$  content only marginally higher.

The  $\text{PdAu}$  NPs had average sizes ranging from 2.6 to 4.8 nm; the average size was found to gradually increase for more  $\text{Au}$  rich NPs (Fig. 1). The pure  $\text{Pd}$  NPs ( $\text{Pd}_{100}\text{Au}_0$ ) were of a similar size (3.8 nm, Fig. 1d) and the TEM images of the NPs confirmed cuboctahedra-like morphology with good monodispersity.

A clear  $\text{Pd}$  oxidation signal (336.7 eV) was observed for  $\text{Pd}$ -rich NPs

by XPS, whereas none was observed in the  $\text{Au}$ -rich NPs ( $\text{Pd}_8\text{Au}_{92}$  NPs, Fig. 2a). Specifically, a larger proportion of  $\text{Pd}$  was found in the  $\text{Pd}(\text{II})$  oxidation state relative to  $\text{Pd}(\text{0})$  as the NPs became more  $\text{Pd}$  rich (Table 2), in agreement with reported literature [25]. The  $\text{Pd}(\text{0})$  peak also shifted to lower binding energies in the more gold-rich samples ( $\text{Pd}_{47}\text{Au}_{53}$ ,  $\text{Pd}_{26}\text{Au}_{74}$ ,  $\text{Pd}_8\text{Au}_{92}$ ). The XPS results showed no changes in the  $\text{Au}$  oxidation state, with the exception of a small shift to higher binding energy for  $\text{Au}$ -rich samples ( $\text{Pd}_{26}\text{Au}_{74}$  and  $\text{Pd}_8\text{Au}_{92}$  in Fig. 2b). These results demonstrate the well-known electronic effect of  $\text{Au}$  on the  $\text{Pd}$  oxidation state and d-level density [35–37].

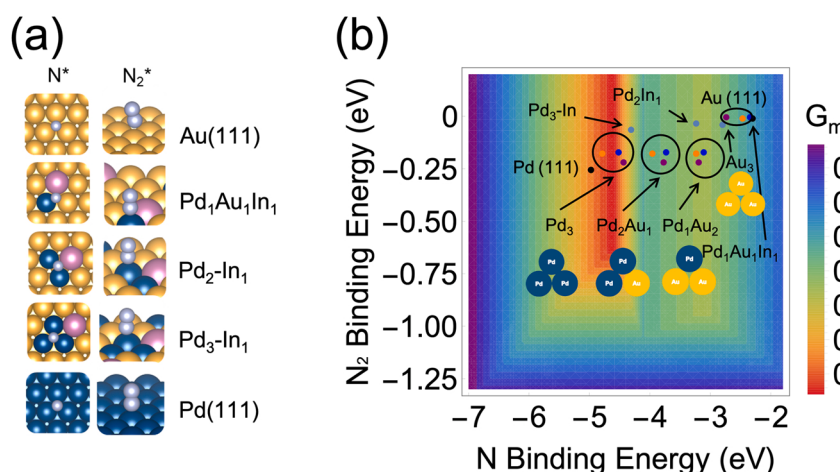
To impart activity for nitrate reduction, the particles were subsequently decorated with  $\text{In}$ . The calculated  $\text{In}$  surface coverage of each of the alloy compositions is shown in Table 3. All samples had  $\text{In}$  surface coverages close to the target value of 25 ( $\pm 3 \text{ sc\%}$ ); the magic cluster model allows us to account for the differences in  $\text{Pd}_x\text{Au}_y$  particle size when determining the proper amount of  $\text{In}$  salt precursor needed to achieve the target  $\text{In}$  content.

Fig. 3 shows the  $\text{Pd} 3\text{d}$ ,  $\text{Au} 4\text{f}$ , and  $\text{In} 3\text{d}$  XPS spectra of the  $\text{In}$ -decorated alloy NPs as a function of alloy composition. There was no obvious shift in the binding energy levels of either  $\text{Pd}$  or  $\text{Au}$  after  $\text{In}$  deposition on any of core materials, relative to the uncoated samples (Fig. 2). The ratio of  $\text{Pd}(\text{0})/\text{Pd}(\text{II})$  of each  $\text{In}$ -decorated  $\text{PdAu}$  NP was consistent and similar with the bimetallic  $\text{PdAu}$  NP analogue. Finally, no binding shift was observed in the  $\text{In}$  ( $\text{In}_2\text{O}_3 \sim 444.3 \text{ eV}$  [38]) regardless of core material, indicating surface  $\text{In}$  of all the  $\text{In}$ -on- $\text{PdAu}$  NPs are electronically similar under *ex situ* characterization conditions.

#### 3.2. Catalytic $\text{NO}_3^-$ reduction performance

The decrease in nitrate concentration fit well to a pseudo first-order model, and apparent observed reaction rate constants were determined from  $\text{NO}_3^-$  reduction concentration-time profiles. To gain a better understanding of the roles of the catalytic sites, we additionally normalized to the total  $\text{PdIn}$  loading of each catalyst, accounting for the inactivity of  $\text{Au}$  [22,39]. Fig. 4a shows typical concentration-time profiles of the catalysts for nitrate reduction, while Fig. 4b shows the resultant pseudo-first order rate constants as a function of core particle composition.

It is clear (Fig. 4b) that the activity of  $\text{In}$ -on- $\text{PdAu}$  NPs had a volcano-shaped dependence on the ratio of  $\text{Pd}:\text{Au}$ , with more  $\text{Pd}$ -rich samples generally exhibiting higher activity. A peak in activity was observed over the  $\text{In}$ -on- $\text{Pd}_{80}\text{Au}_{20}$  NPs with  $k_{\text{cat}} = 7.2 \text{ L/g}_{\text{total (Pd+In)}}/\text{min}$ , which is 2.7 times higher than that observed over the bimetallic  $\text{In}$ -on- $\text{Pd}$  NPs ( $2.7 \text{ L/g}_{\text{total (Pd+In)}}/\text{min}$ ). We note that using metal prices for  $\text{Pd}$  and  $\text{Au}$  of  $\$70.3/\text{g}$  and  $\$59.9/\text{g}$  respectively spot checked on 11/16/2021 the  $\text{In}$ -on- $\text{Pd}_{80}\text{Au}_{20}$  NPs represent a  $2.4 \times$  improvement in cost/performance. It should be noted that all of the trimetallic compositions tested



**Fig. 7.** (a) Binding sites considered in our DFT calculations. (b) Volcano activity plot of nitrite reduction, with the plotted ensembles of  $\text{InPdAu}$ ,  $\text{PdAu}$ , and pure  $\text{Pd}$  and  $\text{Au}$  (111) (black marks). Orange, blue, and purple marks represent  $\text{Pd}_{75}\text{Au}_{25}$ ,  $\text{Pd}_{50}\text{Au}_{50}$ , and  $\text{Pd}_{25}\text{Au}_{75}$ , respectively. Gray marks represent the  $\text{InPdAu}$  systems. Yellow, blue, pink, and light blue spheres represent  $\text{Au}$ ,  $\text{Pd}$ ,  $\text{In}$ , and  $\text{N}$ , respectively. (For interpretation of the references to colour in this figure legend, the reader is referred to the web version of this article.)

here were significantly more active in  $\text{NO}_3^-$  reduction than the analogous bimetallic In-on-Pd NPs, despite Au being catalytically inactive for this reaction. Excessive Au loading was not beneficial to  $\text{NO}_3^-$  reduction reaction, which may be because  $\text{H}_2 \rightarrow \text{H}$ -atom dissociation was impeded over the Au-rich catalysts. The  $\text{H}_2$  activation step is important in this reaction, as the hydrogen adatoms have the two roles of reducing surface N-species and regenerating the oxidized In sites [40].

Fig. 5a & b shows the corresponding concentration profile of intermediate  $\text{NO}_2^-$  and byproduct  $\text{NH}_4^+$  respectively for the In-on-PdAu NP and bimetallic In-on-Pd NP catalysts. As expected, in all cases the concentration of intermediate nitrite increases before decreasing, while ammonium steadily increases over time.

Fig. 5c & d show the selectivity of nitrite and ammonium respectively as a function of nitrate conversion, which is a more rigorous way to compare the catalysts, while Fig. 5e & f show the selectivity to nitrite and ammonia as a function of catalyst composition at low and high nitrate conversion. As can be seen from Fig. 5e & f, at both high and low conversions the selectivity of the trimetallic catalysts is low (<6%), while the bimetallic catalyst forms more nitrite in both cases. Additionally, while the selectivity for ammonium over the trimetallic catalysts is generally low early in the reaction (Fig. 5e), a much different picture emerges at higher conversions. As shown in Fig. 5f the selectivity to ammonium generally decreases with increasing Pd content up to the bimetallic control, where the selectivity sharply rises.

For the Au-rich samples, we suggest that the dilution of the Pd with more Au geometrically isolates Pd sites, decreasing the likelihood of N-N coupling and steering selectivity toward over-hydrogenation to  $\text{NH}_4^+$ . We note that there may be an electronic effect as well; as shown in Fig. 2a & 3a, the most Au-rich samples exhibit a slightly negative shift in Pd binding energies, which is reflective of electron enrichment of Pd. Previous studies have indicated electron-rich Pd favors the over-reduction to ammonia [41,42]. We note that the bimetallic control has higher ammonium selectivity compared to our previous study [20], presumably due to the smaller particle size used in this study. Smaller particles have more low-coordinated metal sites (i.e., edges and corners) which impede nitrogen-containing surface species from coupling to eventually form  $\text{N}_2$  [43]. Still, we note that the bimetallic catalyst alone shows significant improvement compared to previous studies which showed more than 20% selectivity to ammonium [44–46]. Less  $\text{NO}_2^-$  was formed on the Pd-Au surface and was consumed quickly during the reaction (Fig. 5c). Au-diluted Pd surfaces were shown to be beneficial for intermediate  $\text{NO}_2^-$  reduction and so as promoted the pairing of N-species to form  $\text{N}_2$  [25,39].

### 3.3. Potential origins of Au promotion

To better understand the role of Au addition in the nitrate hydroxylation, we also tested the catalysts for  $\text{NO}_2^-$  reduction activity. The initial  $\text{NO}_2^-$  concentration was 37 ppm, consistent with the N-mg/L used for the  $\text{NO}_3^-$  reduction experiments. Fig. 6 shows the pseudo-first order nitrite reduction rate constant plotted against the nitrate reduction rate constant. Monometallic Pd NPs are slightly more active than the bimetallic In-on-Pd NPs (25% sc), which could be due to the blockage of Pd sites active for nitrite reduction and  $\text{H}_2$  dissociation by the In atoms, which are thought to be only active in the  $\text{NO}_3^- \rightarrow \text{NO}_2^-$  step [20,31,47,48].

Further shown in Fig. 6 is that the addition of Au affords up to a two-fold enhancement in nitrite reduction activity. Interestingly, there is a linear relationship between the two reduction rate constants, which suggests the promotional effect is due to the same phenomenon. Moreover, the wider horizontal spread of the data points suggests that nitrite is relatively structure insensitive compared to nitrate, which suggests that only a small number of Pd surface atoms are required for  $\text{NO}_2^-$  reduction reaction [49].

To better understand our experimental results, DFT calculations were performed to calculate the N and  $\text{N}_2$  binding energies at three-fold

ensembles on the InPdAu surfaces (Fig. 7a). These calculations are used together with the volcano activity model of nitrite reduction developed by our previous study [24] to understand the experimentally observed catalytic activity. Fig. 7b shows the derived volcano activity plot for the  $\text{N}_2$  formation pathways, with the free energy barrier of the rate-limiting step,  $G_{max}$ , plotted as the contours. The volcano activity plot is calculated as a function of the N and  $\text{N}_2$  binding energies. The reaction site of a close-packed surface at the peak of the volcano indicates an optimal theoretical activity for nitrite reduction, with the lowest estimated reaction free energy as the rate-determining step. Our previous computational and experimental studies have shown that this volcano activity plot as a function of the N and  $\text{N}_2$  binding energies can effectively predict nitrite reduction activity for transition metal systems [24, 50,51]. For a catalytic reaction at alloy surfaces, the ensemble effect (specific composition of a binding site) is usually dominant for many of the Pd-based systems, since the adsorbate binding is primarily determined by the specific adsorption environment of a surface site [52].

Interestingly, it can be seen that mixing In with Pd (gray mark:  $\text{Pd}_3\text{In}$ ) leads to slightly lower nitrite reduction activity, compared to pure Pd(111) (black mark, Fig. 7b), which indicates that the addition of In inhibits nitrite reduction, in excellent agreement with our experiments (Fig. 6). The three surfaces with different compositions of PdAu with four typical triatomic ensembles were examined and compared with Pd(111), using the calculated binding energies previously published [24]. It can be clearly seen that Pd-rich ensembles (e.g.,  $\text{Pd}_3$ ) are the most active ensembles for nitrite reduction on these Pd-related systems, but the alloying effect of Au can further tune the activity of these Pd-rich sites [23,24]. From these results, it is clear that alloying Au with Pd can help to further promote the activity of nitrite reduction: the compositions of  $\text{Pd}_{50}\text{Au}_{50}$  (blue marks) and  $\text{Pd}_{75}\text{Au}_{25}$  (orange marks) shift the pure Pd ensembles even closer to the peak of volcano, suggesting a promotion effect for nitrite reduction activity presumably due to the electronic and strain effects [52]. Additionally, Au-rich samples ( $\text{Pd}_{25}\text{Au}_{75}$ ) have a reduced enhancement on nitrite reduction activity, likely due to the proportional decrease in the Pd-rich ensembles on surface. As found previously for the bimetallic PdIn [20], the addition of In (gray marks, Fig. 7b) to PdAu ensembles offers no significant enhancement for nitrite reduction. These DFT results are in good agreement with our experimental results that combining In with Pd leads to slightly lower nitrite reduction than pure Pd, while adding Au to Pd can significantly improve nitrite reduction activity (Fig. 6).

The faster nitrite reaction rate over the In-on PdAu catalyst suggests that, for the more complex nitrate reaction, N-fragments are more efficiently cleared (i.e., by more rapid formation of either  $\text{N}_2$  or  $\text{NH}_4^+$ ) from the In-on-PdAu surface compared to the In-on-Pd surface. The Pd sites of the PdAu alloy are occupied to a lesser extent by the N-fragments, implying more sites are available for  $\text{H}_2$  dissociative adsorption. It was previously reported that high occupancy of surface sites by NO fragments (from high nitrite concentrations) leads to self-poisoning of Pd catalysts by blocking  $\text{H}_2$  adsorption [43]. The higher nitrate activity over the In-on-PdAu surface may also be due to more rapid spillover of H adatoms to the In sites, leading to their faster regeneration. Indeed, H-adatoms have previously been shown to be more mobile over PdAu alloys relative to monometallic Pd [24,52]. Additionally, the less occupied Pd sites (of In-on-PdAu) would assist in the spillover of  $\text{NO}_2$  fragments from In sites after reduction of the nitrate species. This is consistent with the selectivity data of Fig. 5e and f, which shows less nitrite intermediate is formed over the In-on-PdAu NPs compared to the bimetallic NPs. Overall, the catalytic reduction of nitrate is plausibly accelerated by improving the activity of the underlying surface (i.e., alloying Pd with Au) rather than the activity of the promoter metal (i.e. In).

### 3.4. Nitrate reduction performance in simulated drinking water

To explore potential applicability in real systems, we tested the In-

on-PdAu trimetallic catalysts using simulated drinking water (SDW) in place of DI water. The normalized pseudo-first-order rate constants were found to be lower (by at least 33%) than those obtained for the catalysts in the DI water (Fig. 4b). The addition of other ions competitively adsorb to the NP surfaces, thus blocking adsorption sites for incoming  $\text{NO}_3^-$  and/or  $\text{H}_2$ , resulting in lower overall reduction activity [21,53]. In SDW, the In-on-Pd<sub>79</sub>Au<sub>21</sub> retained 25% of its DI-water activity (7.2 L/min/g<sub>Pd</sub> in). The Au-rich samples (In-on-Pd<sub>26</sub>Au<sub>74</sub> and In-on-Pd<sub>8</sub>Au<sub>92</sub>), which were less active than In-on-Pd NPs in DI water, were affected the least, retaining 38% of its activity in SDW. These results indicate that a small amount of Au intermixed with the Pd core increases the catalytic denitrification activity of In-on-Pd in realistic water, suggesting the Au imparts deactivation resistance towards cosolutes, as reported by us and others [25,54,55].

#### 4. Conclusions

We synthesized an array of In-decorated PdAu NP catalysts and tested them for nitrate/nitrite reduction ability relative to a bimetallic In-on-Pd NP control. Au generally afforded excellent promotion for nitrate reduction with good selectivity to the desired dinitrogen end product, with ~20 at% Au improving activity by 2.7 times over the non-gold-containing catalyst. DFT calculations indicated that nitrite reduction has the lowest free energies over Pd-rich ensembles, in agreement with the experimental results. We suggest that these sites indirectly promote nitrate reduction as they are better cleared of N-surface fragments, which allows for more facile  $\text{H}_2$  activation responsible for In site regeneration. Finally, experiments in SDW showed that the PdAu alloy core offers protection from deactivation by other species. However, the results also indicate that catalyst deactivation is possible over high concentration of co-contaminants, and further work is needed to probe fouling/deactivation mechanisms.

#### CRediT authorship contribution statement

**Sujin Guo:** Conceptualization, Methodology, Investigation, Validation, Writing. **Hao Li:** Conceptualization, Methodology, Formal analysis, Investigation, Validation, Writing. **Kimberly N. Heck:** Conceptualization, Methodology, Writing. **Xinying Luan:** Investigation, Validation. **Wenhua Guo:** Resources. **Graeme Henkelman:** Conceptualization, Methodology, Investigation, Validation, Writing, Resources, Supervision, Funding. **Michael S. Wong:** Conceptualization, Methodology, Investigation, Validation, Writing, Resources, Supervision, Funding.

#### Declaration of Competing Interest

The authors declare that they have no known competing financial interests or personal relationships that could have appeared to influence the work reported in this paper.

#### Acknowledgement

M.S.W. and S.G. acknowledge partial financial support from the NSF Nanosystems Engineering Research Center for Nanotechnology-Enabled Water Treatment (EEC-1449500) and the China Scholarship Council. The calculations by H.L. and G.H. were supported by the Welch Foundation (F-1841) and the Texas Advanced Computing Center. We dedicate this work in memory of our friend, Dr. Maria Flytzani-Stephanopoulos.

#### Appendix A. Supporting information

Supplementary data associated with this article can be found in the online version at [doi:10.1016/j.apcatb.2021.121048](https://doi.org/10.1016/j.apcatb.2021.121048).

#### References

- [1] N. Kazakis, I. Matiatis, M.M. Ntona, M. Bannenberg, K. Kalaitzidou, E. Kaprara, M. Mitrakas, A. Ioannidou, G. Vargemezis, K. Voudouris, Origin, implications and management strategies for nitrate pollution in surface and ground waters of Anthemountain basin based on a  $\delta^{15}\text{N-NO}_3^-$  and  $\delta^{18}\text{O-NO}_3^-$  isotope approach, *Sci. Total Environ.* (2020), <https://doi.org/10.1016/j.scitotenv.2020.138211>.
- [2] Y. Zhang, P. Shi, J. Song, Q. Li, Application of nitrogen and oxygen isotopes for source and fate identification of nitrate pollution in surface water: a review, *Appl. Sci.* (2018), <https://doi.org/10.3390/app9010018>.
- [3] F.T. Wakida, D.N. Lerner, Non-agricultural sources of groundwater nitrate: a review and case study, *Water Res.* 39 (2005) 3–16, <https://doi.org/10.1016/j.watres.2004.07.026>.
- [4] A.H. Mahvi, J. Nouri, A.A. Babaei, R. Nabizadeh, Agricultural activities impact on groundwater nitrate pollution, *Int. J. Environ. Sci. Technol.* 2 (2005) 41–47.
- [5] L. Knobeloch, B. Salna, A. Hogan, J. Postle, H. Anderson, Blue babies and nitrate-contaminated well water, *Environ. Health Perspect.* 108 (2000) 675–678, <https://doi.org/10.1289/ehp.0010875>.
- [6] N.S. Bryan, H. van Grinsven, The role of nitrate in human health, *Adv. Agron.* 119 (2013) 153–182, <https://doi.org/10.1016/B978-0-12-407247-3.00003-2>.
- [7] M.H. Ward, R.R. Jones, J.D. Brender, T.M. de Kok, P.J. Weyer, B.T. Nolan, C. M. Villanueva, S.G. van Breda, Drinking water nitrate and human health: An updated review, *Int. J. Environ. Res. Public Health* (2018), <https://doi.org/10.3390/ijerph15071557>.
- [8] J. Beauvais, Renewed Call to Action to Reduce Nutrient Pollution and Support for Incremental Actions to Protect Water Quality and Public Health, *State Environ. Comm.* S. W. D., Ed. U.S. Environ. Prot. Agency Washginton, D.C. (2016) 6.
- [9] M.J. Pennino, J.E. Compton, S.G. Leibowitz, Trends in drinking water nitrate violations across the United States, *Environ. Sci. Technol.* (2017), <https://doi.org/10.1021/acs.est.7b04269>.
- [10] S.K. Sharma, R.C. Sobti, Nitrate removal from ground water: a review, *E-J. Chem.* 9 (2012) 1667–1675, <https://doi.org/10.1155/2012/154616>.
- [11] D. Clifford, X. Liu, Ion exchange for nitrate removal, *J. Am. Water Work. Assoc.* (1993), <https://doi.org/10.1002/j.1551-8833.1993.tb05971.x>.
- [12] K.P. Fedinick, Mp. Mae Wu, M. Panditharatne, Erik D. Olson, Threats on tap: widespread violations highlight need for investment in water infrastructure and protections, 2017.
- [13] S. Hörlöd, K.-D. Vorlop, T. Tacke, M. Sell, Development of catalysts for a selective nitrate and nitrite removal from drinking water, *Catal. Today* 17 (1993) 21–30, [https://doi.org/10.1016/0920-5861\(93\)80004-K](https://doi.org/10.1016/0920-5861(93)80004-K).
- [14] K.J. Reddy, J. Lin, Nitrate removal from groundwater using catalytic reduction, *Water Res.* (2000), [https://doi.org/10.1016/S0043-1354\(99\)00227-4](https://doi.org/10.1016/S0043-1354(99)00227-4).
- [15] K.N. Heck, S. Garcia-Segura, P. Westerhoff, M.S. Wong, Catalytic converters for water treatment, *Acc. Chem. Res.* 52 (2019) 906–915.
- [16] A. Garron, F. Epron, Use of formic acid as reducing agent for application in catalytic reduction of nitrate in water, *Water Res.* 39 (2005) 3073–3081, <https://doi.org/10.1016/j.watres.2005.05.012>.
- [17] A. Pintar, J. Batista, J. Levec, T. Kajuchi, Kinetics of the catalytic liquid-phase hydrogenation of aqueous nitrate solutions, *Appl. Catal. B Environ.* 11 (1996) 81–98, [https://doi.org/10.1016/S0926-3373\(96\)00036-7](https://doi.org/10.1016/S0926-3373(96)00036-7).
- [18] X. Huo, D.J. Van Hoomissen, J. Liu, S. Vyas, T. Strathmann, Hydrogenation of aqueous nitrate and nitrite with ruthenium catalysts, *Appl. Catal. B Environ.* 211 (2017) 188–198, <https://doi.org/10.1016/j.apcatb.2017.04.045>.
- [19] R. Zhang, D. Shuai, K. a Guy, J.R. Shapley, T.J. Strathmann, C.J. Werth, Elucidation of nitrate reduction mechanisms on a pd-in bimetallic catalyst using isotope labeled nitrogen species, *ChemCatChem* 5 (2013) 313–321, <https://doi.org/10.1002/cctc.201200457>.
- [20] S. Guo, K. Heck, S. Kasiraju, H. Qian, Z. Zhao, L.C. Grabow, J.T. Miller, M.S. Wong, Insights into nitrate reduction over indium-decorated palladium nanoparticle catalysts, *ACS Catal.* 8 (2018) 503–515.
- [21] S. Guo, C.D. Powell, D. Villagran, M.S. Wong, Magnetic In-Pd catalysts for nitrite degradation, *Environ. Sci. Nano.* (2020).
- [22] W.C. Elias, K.N. Heck, S. Guo, S. Yazdi, C. Ayala, S.S. Grossweiler, J.B. Domingos, E. Ringe, M.S. Wong, Indium-decorated Pd nanoparticles degrade nitrate anions rapidly, *Appl. Catal. B Environ.* (2020), 119048.
- [23] H. Qian, Z. Zhao, J.C. Velazquez, L.A. Pretzer, K.N. Heck, M.S. Wong, Supporting palladium metal on gold nanoparticles improves its catalysis for nitrite reduction, *Nanoscale* 6 (2014) 358–364.
- [24] H. Li, S. Guo, K. Shin, M.S. Wong, G. Henkelman, Design of a Pd-Au nitrite reduction catalyst by identifying and optimizing active ensembles, *ACS Catal.* (2019), <https://doi.org/10.1021/acscatal.9b02182>.
- [25] S. Seraj, P. Kunal, H. Li, G. Henkelman, S.M. Humphrey, C.J. Werth, PdAu alloy nanoparticle catalysts: effective candidates for nitrite reduction in water, *ACS Catal.* 7 (2017) 3268–3276, <https://doi.org/10.1021/acscatal.6b03647>.
- [26] L.C. Green, D.A. Wagner, J. Glogowski, P.L. Skipper, J.S. Wishnok, S. R. Tannenbaum, Analysis of nitrate, nitrite, and  $[15\text{N}]$ nitrate in biological fluids, *Anal. Biochem.* 126 (1982) 131–138, [https://doi.org/10.1016/0003-2697\(82\)90118-X](https://doi.org/10.1016/0003-2697(82)90118-X).
- [27] NSF/ANSI 53 Standards for Water Treatment Systems, (n.d.).
- [28] P. Kunal, H. Li, B.L. Dewing, L. Zhang, K. Jarvis, G. Henkelman, S.M. Humphrey, Microwave-assisted synthesis of Pd<sub>x</sub>Au<sub>100-x</sub> alloy nanoparticles: a combined experimental and theoretical assessment of synthetic and compositional effects upon catalytic reactivity, *ACS Catal.* 6 (2016) 4882–4893, <https://doi.org/10.1021/acscatal.6b01014>.
- [29] T. Teranishi, M. Miyake, Size control of palladium nanoparticles and their crystal structures, *Chem. Mater.* (1998), <https://doi.org/10.1021/cm9705808>.

[30] U. Prüsse, M. Hählein, J. Daum, K.-D. Vorlop, Improving the catalytic nitrate reduction, *Catal. Today* 55 (2000) 79–90.

[31] B.P. Chaplin, J.R. Shapley, C.J. Werth, The selectivity and sustainability of a Pd-In/γ-Al<sub>2</sub>O<sub>3</sub> catalyst in a packed-bed reactor: The effect of solution composition, *Catal. Lett.* 130 (2009) 56–62, <https://doi.org/10.1007/s10562-009-9883-4>.

[32] J.P. Perdew, K. Burke, M. Ernzerhof, Generalized gradient approximation made simple, *Phys. Rev. Lett.* 77 (1996) 3865–3868, <https://doi.org/10.1103/PhysRevLett.77.3865>.

[33] P.E. Blöchl, Projector augmented-wave method, *Phys. Rev. B* 50 (1994) 17953–17979, <https://doi.org/10.1103/PhysRevB.50.17953>.

[34] H.J. Monkhorst, J.D. Pack, Special points for Brillouin-zone integrations, *Phys. Rev. B* (1976), <https://doi.org/10.1103/PhysRevB.13.5188>.

[35] Z. Zhao, J.T. Miller, T. Wu, N.M. Schweitzer, M.S. Wong, EXAFS characterization of palladium-on-gold catalysts before and after glycerol oxidation, *Top. Catal.* 58 (2015) 302–313, <https://doi.org/10.1007/s11244-015-0371-3>.

[36] L.A. Pretzer, H.J. Song, Y.-L. Fang, Z. Zhao, N. Guo, T. Wu, I. Arslan, J.T. Miller, M.S. Wong, Hydrodechlorination catalysis of Pd-on-Au nanoparticles varies with particle size, *J. Catal.* 298 (2013) 206–217.

[37] Z. Zhao, K.N. Heck, P. Limpornipat, H. Qian, J.T. Miller, M.S. Wong, Hydrogen-generating behavior of Pd-decorated gold nanoparticles via formic acid decomposition, *Catal. Today* (2018).

[38] C.J.P. Alexander V. Naumkin, Anna Kraut-Vass, Stephen W. Gaarenstroom, NIST X-ray Photoelectron Spectroscopy Database, Version 4.1, (2012).

[39] H. Qian, Z. Zhao, J. Velazquez, L. Pretzer, Supporting palladium metal on gold nanoparticles improves its catalysis for nitrite reduction, *Nanoscale* (2014) 358–364, <https://doi.org/10.1039/c3nr04540d>.

[40] L. Kuai, Z. Chen, S. Liu, E. Kan, N. Yu, Y. Ren, C. Fang, X. Li, Y. Li, B. Geng, Titania supported synergistic palladium single atoms and nanoparticles for room temperature ketone and aldehydes hydrogenation, *Nat. Commun.* (2020), <https://doi.org/10.1038/s41467-019-13941-5>.

[41] J.P. Dacquin, S. Troncée, V.I. Parvulescu, P. Granger, Unexpected kinetic behavior of structured Pd/CeO<sub>2</sub>-ZrO<sub>2</sub> toward undesired ammonia formation and consumption during nitrites reduction: role of the reactivity of oxygen from ceria, *Catal. Today* (2020), <https://doi.org/10.1016/j.cattod.2020.05.054>.

[42] M.S. Kim, S.H. Chung, C.J. Yoo, M.S. Lee, I.H. Cho, D.W. Lee, K.Y. Lee, Catalytic reduction of nitrate in water over Pd-Cu/TiO<sub>2</sub>catalyst: effect of the strong metal-support interaction (SMSI) on the catalytic activity, *Appl. Catal. B Environ.* 142–143 (2013) 354–361, <https://doi.org/10.1016/j.apcatb.2013.05.033>.

[43] D. Shuai, D.C. McCalman, J.K. Choe, J.R. Shapley, W.F. Schneider, C.J. Werth, Structure sensitivity study of waterborne contaminant hydrogenation using shape- and size-controlled Pd nanoparticles, *ACS Catal.* 3 (2013) 453–463, <https://doi.org/10.1021/cs300616d>.

[44] J. Jung, S. Bae, W. Lee, Nitrate reduction by maghemite supported Cu-Pd bimetallic catalyst, *Appl. Catal. B Environ.* 127 (2012) 148–158, <https://doi.org/10.1016/j.apcatb.2012.08.017>.

[45] O.S.G.P. Soares, J.J.M. Orfão, M.F.R. Pereira, Bimetallic catalysts supported on activated carbon for the nitrate reduction in water: optimization of catalysts composition, *Appl. Catal. B Environ.* (2009), <https://doi.org/10.1016/j.apcatb.2009.06.013>.

[46] A. Devadas, S. Vasudevan, F. Epron, Nitrate reduction in water: Influence of the addition of a second metal on the performances of the Pd/CeO<sub>2</sub> catalyst, *J. Hazard. Mater.* (2011), <https://doi.org/10.1016/j.jhazmat.2010.10.063>.

[47] Z. Gao, Y. Zhang, D. Li, C.J. Werth, Y. Zhang, X. Zhou, Highly active Pd-In/ mesoporous alumina catalyst for nitrate reduction, *J. Hazard. Mater.* 286 (2015) 425–431, <https://doi.org/10.1016/j.jhazmat.2015.01.005>.

[48] B.P. Chaplin, M. Reinhard, W.F. Schneider, C. Schüth, J.R. Shapley, T. J. Strathmann, C.J. Werth, Critical review of Pd-based catalytic treatment of priority contaminants in water, *Environ. Sci. Technol.* 46 (2012) 3655–3670, <https://doi.org/10.1021/es204087q>.

[49] K.A. Guy, H. Xu, J.C. Yang, C.J. Werth, J.R. Shapley, Catalytic nitrate and nitrite reduction with Pd-Cu/PVP colloids in water: composition, structure, and reactivity correlations, *J. Phys. Chem. C* 113 (2009) 8177–8185, <https://doi.org/10.1021/jp810049y>.

[50] J.P. Troutman, H. Li, A.M. Haddix, B.A. Kienzle, G. Henkelman, S.M. Humphrey, C. J. Werth, PdAg alloy nanocatalysts: toward economically viable nitrite reduction in drinking water, *ACS Catal.* (2020), <https://doi.org/10.1021/acscatal.0c01538>.

[51] H. Li, C. Yan, H. Guo, K. Shin, S.M. Humphrey, C.J. Werth, G. Henkelman, CuIr<sub>1-x</sub> nanoalloy catalysts achieve near 100% selectivity for aqueous nitrite reduction to NH<sub>3</sub>, *ACS Catal.* (2020), <https://doi.org/10.1021/acscatal.0c01604>.

[52] H. Li, K. Shin, G. Henkelman, Effects of ensembles, ligand, and strain on adsorbate binding to alloy surfaces, *J. Chem. Phys.* 149 (2018), <https://doi.org/10.1063/1.5053894>.

[53] C. Lee, S. Guo, H. Rho, J. Levi, S. Garcia-Segura, M.S. Wong, J. Gardea-Torresdey, P. Westerhoff, Unified Metallic Catalyst Aging Strategy and Implications for Water Treatment, *Environ. Sci. Technol.* (n.d.).

[54] K.N. Heck, M.O. Nutt, P. Alvarez, M.S. Wong, Deactivation resistance of Pd/Au nanoparticle catalysts for water-phase hydrodechlorination, *J. Catal.* 267 (2009) 97–104.

[55] Y. Ben Yin, C.L. Coonrod, K.N. Heck, I.A. Said, C.D. Powell, S. Guo, M.A. Reynolds, M.S. Wong, Room-temperature catalytic treatment of high-salinity produced water at neutral pH, *Ind. Eng. Chem. Res.* (2020), <https://doi.org/10.1021/acs.iecr.0c00521>.